Importance of multiscale analysis in HARDI studies

I. Kezele[1], C. Poupon[1], M. Descoteaux[1], F. Poupon[1], and J-F. Mangin[1]
[1]NeuroSpin, CEA, Saclay, France

Introduction and Background. High angular resolution distribution diffusion imaging (HARDI) implicitly captures information about the structure in which the diffusion process takes place. HARDI allows examination of relatively wide range of diffusion signal angular frequencies that, due to the complexity of both diffusion process and its milieu, may spread over multiple bands. In consequence, we opt for multiscale analysis, probing all frequencies, but also favouring those frequencies that are more in concordance with our specific aims, which are to deduce and sharpen fibre distributions. Inherent HARDI signal sphericity motivated us to take on the concepts of multiscale spherical wavelet analysis. Since the directions of maximal diffusion are unknown a priori, HARDI explores the space in uniform manner, and thus suffers from a certain amount of information redundancy. HARDI projections onto predefined bases, like spherical harmonics (SHs)[1-4] can reduce the signal complexity, but are often not fully adapted to the problem at hand (e.g., fibre orientation distribution (FOD) sparsity). Deconvolution methods for FOD estimation [5,6], probe the signal locally, allowing for sparse representation, but are highly susceptible to noise. Nonetheless, they work quite well even at low b-values. Recently, an elegant framework for HARDI multiscale, ridgelet analysis was derived [7], reducing the signal representation to as little as 10 basis functions. We propose to denoise and sharpen the orientation distribution function (ODF) directly [8]. The algorithm that we employ is based on the spherical version of "à trous" algorithm [9], using B3-spline scaling function (defined in Fourier space). Using Funk-Radon relation between ODF and HARDI signal, we define a framework to probe HARDI signal directly and obtain a sparse and sharp representation of angular content of diffusion. Herein, we would like to stress the importance of multiscale signal analysis (through illustrative examples), and to show applications to real data, with as little as 64 directions, and b-value of 1000 s/mm².

Methods. *Image Acquisition*. Physical phantoms, emulating two fibre bundles crossing at 45° and 90° [10] were acquired on a 1.5T Signa MR system (GE Healthcare, Milwaukee), TE/TR =130ms/4.5s,12.0s (45° and 90° phantom, respectively), BW=200KHz. FOV = 32cm, matrix size of 32x32), b = 2000s/mm², 4000 uniformly distributed orientations SNRmin > 4. The first real dataset was acquired on the same scanner. Twice refocused DW-SS-SE-EPI (TE/TR=100.2ms/19s, BW=200KHz, FOV=24cm on a 128x128 matrix, TH=2mm, 60 axial slices) was employed to obtain T2-weighted (b=0) and HARDI (b=3000s/mm², 200 directions) data of a healthy volunteer (publicly available HARDI database [11]). The second real data set was acquired on 3T Trio MR system (Siemens, Erlangen). Parallel imaging with GRAPPA factor of 2 (TE/TR=147ms/11,5s, BW=1680Hz/pixel, 96x96 matrix, resolution 2x2x2mm^3, 60 axial slices) was employed to obtain T2-weighted (b=0) and HARDI (b=1000s/mm², 64 directions) data of a healthy volunteer. *ODF wavelet analysis*. In [8], we derived in detail our algorithm for ODF wavelet-based denoising and sharpening. The analysis is redundant, and the frequencies decrease dyadically with increasing scales. The scaling function is spherical B3-spline, and wavelets at each scale are defined as the difference of "lowpass" signal content at two successive scales. The final ODF decomposition amounts to: $\Psi = \Psi_J + \Sigma\omega_j$ (Ψ stands for ODF, Ψ_J for its lowest frequency content and ω_j for its high frequency details, i.e., wavelets at each frequency scale j; j = 0 to J, and J = 2 for the experiments herein). Typically, the frequencies we analyse correspond to SH orders from 2 to 8/16. Since our goal is not only to denoise and shrink the data but also (and very importantly) to amplify its angular frequency content relevant for fibre orientation estimation, we reduce ODF to sharp ODF that is given by: $\Psi_{sharp} = \Sigma\omega_j$.(Note that the maximum SH order of Ψ_J is typically not higher than 2, i.e. it corresponds to a 2nd order tensor, and is not of interest in descriptions of more "exotic" fibre configurations, including crossings, kissings, splits, etc.). The final Ψ_{sharp} is obtained after wavelet reduction at each scale, and is given as a sum of 4 (for 90° phantom) and 10 (for 45° phantom and both real data sets) wavelet coefficients (per scale) with largest magnitudes. Laplace-Beltrami smoothing [4] was used when estimating the SHs (λ =0.006), to render them more stable, especially in real data where SNR was rather low (≅2).

Results. First, we illustrate the method on the phantom data. The purpose is to show how different angular frequency bands capture different information even for controllable geometries, stressing the importance of multiscale analysis. Only with the sum of distinct frequency components can we appreciate the true fibre constellation and (importantly) the proportions between these different compartments. Then, we show the similar findings on real data. Also, on real data, we show some limiting results (i.e., low orientation number, confining the frequency spectrum to those SH orders that can be reliably estimated from such a "reduced" spatial sampling), where the wavelets are shrunk to a single scale. In this limit, multiscale analysis can no longer be performed, nonetheless the wavelet framework can still be used to denoise and sharpen the data, even at a single level.

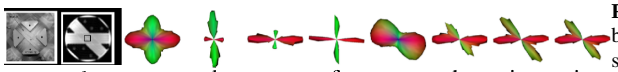

Figure 1. a, c, d, e, f correspond to 90°-crossing and b, f, g, h, i, j to 45°-crossing phantom. For both phantoms from left to right: phantom, SH-analytical ODF (max SH order = 16), lowest scale details (max SH order = 16), second scale details (max SH order = 8), and our sharp ODF. Fort both phantoms, HARDI directions were sub-sampled to 200, uniformly distributed. Note how different scales capture complementary information about fibre distribution. This is in particular prominent for the 90°-crossing phantom, where each scale catches one of the two fibre directions (y and x, respectively).

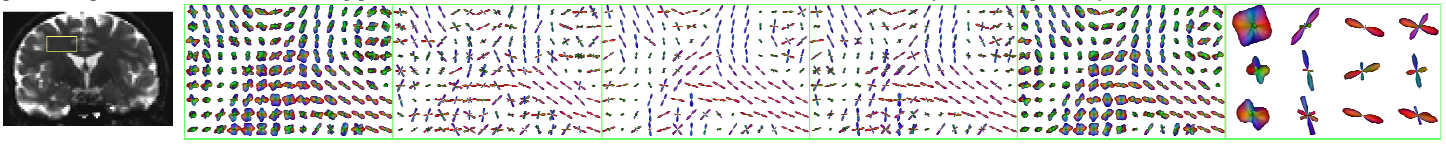

Figure 2. a) Analysed ROI, b) SH-analytical ODF (max SH order = 8), c) lowest scale details (max SH order = 8), d) second scale details (max SH order = 4), e) sharp ODF, f) sum of lowest frequency signal scale (max SH order = 2) and sharp ODF (i.e., overall reconstructed ODF), g) three illustrative examples from white matter of the same ROI (shown are b, c, d and e parts), of how different scales capture complementary information about fibre distribution (i.e., different principal fibre directions in a voxel), and the proportion between different fibre compartments.

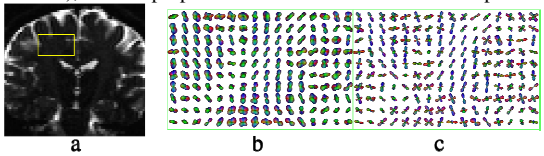

Figure 3. a) Analysed ROI, b) SH-analytical ODF (max SH order = 6), c) lowest scale details (max SH order = 6). In this "degenerate" case, where the wavelet analysis is reduced to a single scale (due to low max SH order, imposed by the small number of directions and stability of SH estimates on noisy data), our Ψ_{sharp} is given by a sum of shrunk wavelet coefficients of the lowest scale only (shown in c).

Discussion. We demonstrated our algorithm to reduce and sharpen ODFs within the framework of spherical wavelet analysis. We showed on phantom and real data that signals are spread over multiple frequency scales, and that different scales capture complementary information about fibre distribution, and the proportion between different fibre compartments (the latter being more important for smaller crossing angles). Thus, we strongly advocate the importance of multiscale analysis of HARDI signals. Also, although for lower angular resolution of acquired HARDI data it is not possible to employ multiscale analysis and significantly reduce the data, spherical wavelets can still be successfully employed to sharpen ODF profiles, as it was seen through the example of the second real data set (Fig. 3).

Bibliography: 1. Frank, L., MRM 47(6) (2002) 1083–1099. 2. D. Alexander, et al. MRM 48(2) (2002) 331–340. 3. C. Hess, et al. MRM 56 (2006) 104–117. 4. M. Descoteaux, et al. MRMedicine 58(3) (2007) 497–510. 5. J.D. Tournier, et al. NIMG 23 (2004) 1176–1185. 6. Tournier, J.D., et al. NIMG 35(4) (2007) 1459–1472. 7. O.V. Michailovich, et al. In IEEE ISBI (2008). 8 I. Kezele, et al. CDMRI08, MICCAI 2008. 9. J.-L Starck, et al. A&A 446 (2006) 1191–1204. 10. Poupon, C., et al. MRM (2008) In press. 11. Poupon, C., et al. In HBM (2006).